The Ndc80 kinetochore complex directly modulates microtubule dynamics

Neil T. Umbreit[a,1], Daniel R. Gestaut[a,1,2], Jerry F. Tien[a,1], Breanna S. Vollmar[a,3], Tamir Gonen[a,b,3], Charles L. Asbury[c], and Trisha N. Davis[a,4]

[a]Department of Biochemistry, [c]Department of Physiology and Biophysics, and [b]Howard Hughes Medical Institute, University of Washington, Seattle, WA 98195

The conserved Ndc80 complex is an essential microtubule-binding component of the kinetochore. Recent findings suggest that the Ndc80 complex influences microtubule dynamics at kinetochores in vivo. However, it was unclear if the Ndc80 complex mediates these effects directly, or by affecting other factors localized at the kinetochore. Using a reconstituted system in vitro, we show that the human Ndc80 complex directly stabilizes the tips of disassembling microtubules and promotes rescue (the transition from microtubule shortening to growth). In vivo, an N-terminal domain in the Ndc80 complex is phosphorylated by the Aurora B kinase. Mutations that mimic phosphorylation of the Ndc80 complex prevent stable kinetochore-microtubule attachment, and mutations that block phosphorylation damp kinetochore oscillations. We find that the Ndc80 complex with Aurora B phosphomimetic mutations is defective at promoting microtubule rescue, even when robustly coupled to disassembling microtubule tips. This impaired ability to affect dynamics is not simply because of weakened microtubule binding, as an N-terminally truncated complex with similar binding affinity is able to promote rescue. Taken together, these results suggest that in addition to regulating attachment stability, Aurora B controls microtubule dynamics through phosphorylation of the Ndc80 complex.

mitosis | Hec1 | single molecule | optical trap | total internal reflection fluorescence microscopy

During mitosis, replicated chromosomes are segregated by the mitotic spindle, a bipolar array of dynamic microtubules. Each chromatid is linked to a bundle of microtubules (a "K-fiber") by a kinetochore. To ensure accurate chromosome segregation, regulatory mechanisms detect and correct errors in attachments between kinetochores and spindle microtubules. The conserved Aurora B kinase plays a crucial role in the resolution of aberrant kinetochore-microtubule attachments (1). Aurora B has many identified targets at the kinetochore, and it is generally thought that phosphorylation of these targets triggers the release of incorrect attachments (2–7). However, emerging evidence suggests that Aurora B activity does not always result in kinetochore-microtubule detachment. For example, early in mitosis when merotelic attachments are more prevalent, phosphorylation of the Ndc80 complex (the key microtubule-binding component of the kinetochore) is relatively high, yet kinetochores do not appear to release from their K-fibers (8, 9). Similarly, syntelic attachments formed in the presence of a reversible Aurora B inhibitor are not immediately released when the kinase is reactivated (10). Instead, the K-fiber microtubules disassemble, carrying the kinetochores back to the centrosome, where the attachments are corrected by an unknown mechanism. These results suggest that Aurora B additionally acts to regulate microtubule dynamics as a part of its mechanism of error correction.

Additional findings suggest that Aurora B modulates microtubule dynamics through regulation of the Ndc80 complex. A component of the Ndc80 complex, the Hec1 protein, has a disordered N-terminal tail that is targeted by Aurora B in vivo (11, 12). In PtK cells, preventing phosphorylation of these target sites not only results in hyperstable kinetochore-microtubule attachments, but also damped kinetochore oscillations (8). The abnormal oscillations could be explained by direct or indirect contributions from the Ndc80 complex. The Ndc80 complex could itself directly control microtubule dynamics in response to Aurora B activity. An alternative (but not mutually exclusive) explanation is that phosphorylation of Hec1 alters the localization of other factors that modulate dynamics. These factors may include the microtubule stabilizer EB1 and the microtubule depolymerase MCAK, both of which are also targets of Aurora B (13–19).

Here, we show that the human Ndc80 complex directly stabilizes the tips of disassembling microtubules, slows the rate of disassembly, and promotes microtubule rescue (the transition from microtubule shortening to growth) in vitro. In contrast, the Ndc80 complex with mutations mimicking Aurora B phosphorylation was impaired in its ability to influence microtubule dynamics, even when tracking with the tips of disassembling microtubules. This diminished ability of the phosphomimetic complex to affect dynamics is not solely a result of weakened microtubule binding, as an N-terminally truncated complex with similar affinity was still able to promote rescue. These results suggest that Aurora B modulates microtubule dynamics through regulation of the Ndc80 complex, and this mechanism could be separable from effects on attachment stability.

Results

Characterization of Full-Length Human Ndc80 Complex. The conserved Ndc80 complex is an essential microtubule-binding component of the kinetochore (20). Although the Ndc80 complex from yeast and worms has been extensively studied in vitro (21–26), most work on the human complex has been limited to the use of truncated forms (26–31). We expressed and purified full-length human Ndc80 complex from *Escherichia coli* for in vitro characterization (Fig. S1). As seen by negative-stain EM, this recombinant Ndc80 complex bound to taxol-stabilized microtubules (Fig. 1A). Using total internal reflection fluorescence (TIRF) microscopy, we visualized single molecules of GFP-tagged Ndc80 complex on taxol-stabilized microtubules (Fig. 1B and Fig. S2) and measured their dissociation and diffusion rate constants ($k_{off} = 0.21 \pm 0.01$ s^{-1}, $D = 0.018 \pm 0.001$ μm$^2 \cdot$s^{-1}) (Fig. 1 C and D). The affinity and cooperativity of microtubule binding were
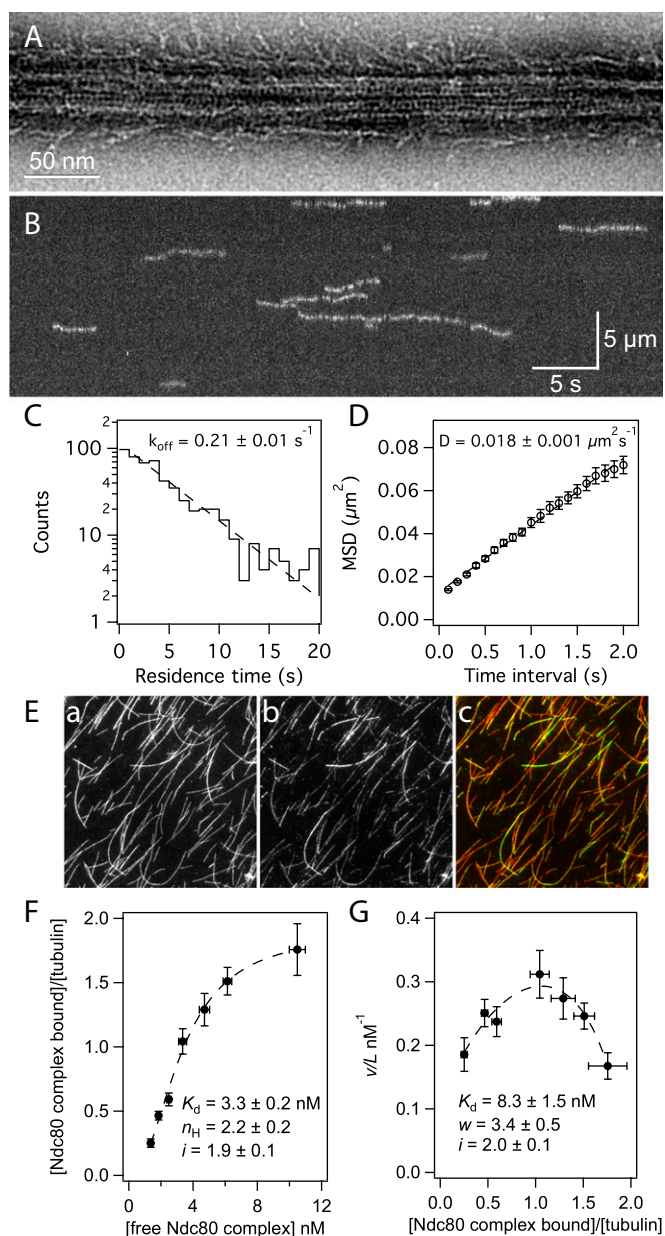
BIOCHEMISTRY

Fig. 1. The human Ndc80 complex binds to and diffuses along the microtubule lattice. (*A*) Negative-stain electron micrograph of the Ndc80 complex on a taxol-stabilized microtubule. (*B*) A representative kymograph showing the binding and diffusion of Ndc80 complex (5 pM complex in solution) on taxol-stabilized microtubules. Position along the microtubule is depicted on the vertical axis over time on the horizontal axis. (*C*) Residence time distributions of GFP-tagged Ndc80 complex on microtubules fit with a single exponential (dashed line) to calculate the off-rate constant, k_{off}. (*D*) Mean-squared displacement (MSD) $\pm$ SEM vs. time lag. A linear fit to the data (dashed line) was used to determine the diffusion constant, *D*. (*C* and *D*) *n* = 584. (*E*) Representative image from the bulk microtubule binding assay with GFP-tagged Ndc80 complex (2 nM) on taxol-stabilized Alexa-568-labeled microtubules (2.5 nM tubulin dimer). Panels show microtubules (a), Ndc80 complex (b), and merge (c). Panel dimensions are 66 by 66 µm. (*F*) Plot of binding density (*v*) versus free Ndc80 complex concentration (*L*). A fit to the Hill model (dashed line) was used to determine the apparent affinity (K_d), Hill coefficient (n_H), and lattice occupancy (*i*, the number of Ndc80 complexes bound per tubulin dimer). (*G*) Scatchard plot of the same data shown in *F*, fit to the McGhee and von Hippel model (dashed line) to calculate the K_d, cooperativity parameter (*w*), and *i*. For *F* and *G*, *n* = 8–10 replicates per data point, markers are mean $\pm$ SEM, and errors on model fit parameters (K_d, n_H, *w*, and *i*) represent SD.

measured using a bulk microtubule binding assay that measures the amount of GFP-tagged complex bound to microtubules over varying concentrations of complex (Fig. 1*E*) (32, 33). Based on a standard Hill model fit (34), the Ndc80 complex binds microtubules with a strong apparent affinity ($K_d = 3.3 \pm 0.2$ nM) and has a Hill coefficient of 2.2 ± 0.2 (Fig. 1*F*). The Hill model describes cooperativity arising from allosteric changes that enhance ligand binding to a protein. In our binding assay, cooperativity is likely based on interactions between Ndc80 complexes that occur when they are bound to microtubules. Therefore, we used a model previously developed by McGhee and von Hippel that describes cooperativity between ligands binding to a polymer lattice (35). Fitting the binding data with this model (Fig. 1*G*) also showed a strong apparent affinity ($K_d = 8.3 \pm 1.5$ nM) and cooperativity between Ndc80 complexes on the microtubule lattice ($w = 3.4 \pm 0.5$). Compared with the Hill model fit, the McGhee and von Hippel model fit yielded a weaker apparent K_d for a single complex. Thus, interactions between complexes bound to the microtubule contribute to the K_d predicted by the Hill model. This finding is supported by the observation that at high concentrations, truncated Ndc80 complex binds microtubules in clusters (28). Fits to both models revealed a lattice occupancy of approximately two Ndc80 complexes per tubulin dimer, consistent with cryo-EM reconstructions that showed a 4-nm spacing of the truncated complex on microtubules (28).

Ndc80 Complex Directly Stabilizes Disassembling Microtubule Tips and Promotes Microtubule Rescue. In vivo, kinetochores transmit forces generated by the mitotic spindle to drive chromosome movement (36). This process depends on the ability of microtubule-binding components of the kinetochore to form stable attachments to dynamic microtubule tips. Using TIRF microscopy, we visualized the GFP-tagged Ndc80 complex on disassembling microtubules. In these assays, microtubule disassembly was induced by the removal of free tubulin. The human Ndc80 complex can track with disassembling microtubule tips (Fig. 2*A*), unlike the budding yeast Ndc80 complex, which requires the Dam1 complex or oligomerization on the surface of beads (23, 24). The human Ndc80 complex also slowed the rate of microtubule disassembly (Fig. 2*C*). As the concentration of the complex was increased from 0 to 500 pM, microtubule disassembly was slowed from 280 ± 20 nm/s to 100 ± 10 nm/s.

At 500 pM, bright particles of GFP-tagged Ndc80 complex were observed on microtubules (Fig. 2*B*), consistent with its cooperative binding behavior in our bulk assays. In some cases, disassembly appeared to stall as the tip reached these particles, and only continued after the Ndc80 complex appeared to detach. This behavior resulted in a step-like appearance in kymographs (Fig. 2*B*). Furthermore, Alexa-647–labeled tubulin decorated with Ndc80 complex was often seen bending away from the long axis of the microtubule (observed for $66 \pm 10\%$ of microtubules) (Fig. 2*D*, Fig. S3 *A and B*, and Movie S1). Because these curled extensions can be resolved by light microscopy (116-nm pixels), their curvature is gentler than the tight 20-nm curls seen at bare disassembling tips by cryo-EM in vitro (37). To further investigate tip structure in the presence of Ndc80 complex, we performed a similar disassembly assay and visualized the microtubule tips by negative-stain EM. We observed open protofilament sheets emanating from the tips of microtubules stabilized by Ndc80 complex (Fig. 2*E*). These sheets were not observed at the tips of microtubules stabilized by taxol or by the Dam1 complex (Fig. S3*C*) (38). Microtubules exposed to the same conditions in the absence of any stabilizing factor completely disassembled into free tubulin. Although we were unable to distinguish between microtubule plus- and minus-ends in the electron micrographs, curled extensions were observed in the presence of Ndc80 complex at both microtubule ends in the TIRF assay (Fig. S3*A*). Together, the TIRF and
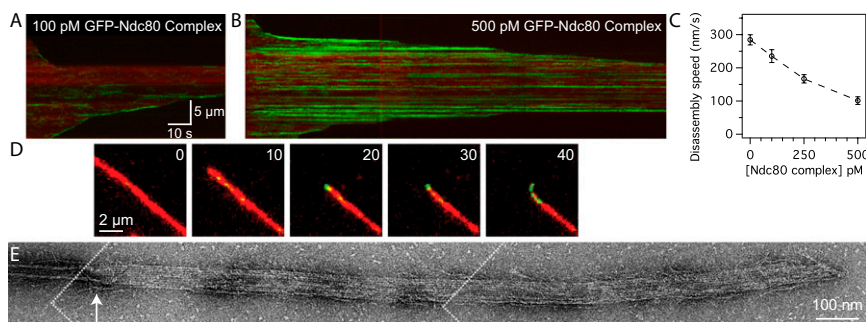
Fig. 2. The Ndc80 complex slows microtubule disassembly and stabilizes protofilament extensions. Kymographs of disassembling microtubules (red) in the presence of (*A*) 100 pM or (*B*) 500 pM GFP-tagged Ndc80 complex (green). Brightness and contrast were adjusted equally in *A* and *B*. (*C*) Mean disassembly speeds ± SEM for microtubules in the presence of increasing concentrations of Ndc80 complex (without Ndc80 complex, n = 80; 100 pM Ndc80 complex, n = 31; 250 pM, n = 29; 500 pM, n = 34). (*D*) Time-lapse images of a disassembling microtubule (red) in the presence of 500 pM GFP-tagged Ndc80 complex (green) as a curled extension formed at the tip. *Inset* numbers show elapsed time, in seconds. See Fig. S3*B* for a gallery of images showing curled extensions. (*E*) Negative-stain electron micrograph of a disassembling microtubule tip (see *SI Materials and Methods*) stabilized by the Ndc80 complex. An arrow marks the transition from a closed microtubule to an open sheet. The figure was constructed from three images, the boundaries of which are depicted by dotted white lines.

EM assays suggest that the Ndc80 complex slows disassembly by stabilizing protofilament extensions at microtubule tips.

To test how purified Ndc80 complex couples to dynamic microtubule tips under force, we used an optical trap-based bead motility assay (39). By incubating 11 pM beads with 5 nM Ndc80 complex (~450 complexes per bead), we estimate that up to ~20 complexes can interact with the microtubule tip based on geometric constraints (23). This number closely approximates the number of Ndc80 complexes per kinetochore microtubule in vivo (40). These beads remained coupled to microtubule tips against 2 pN of tension (Fig. 3 *A* and *B*), similar to the forces sustained by kinetochore-microtubule attachments in vivo, which are estimated to be 0.4–8 pN (23, 41, 42). Against the applied force, beads tracked robustly with the tips of disassembling microtubules over an average distance of 970 ± 190 nm (n = 44). Consistent with results from our TIRF-based assays, microtubule disassembly was slowed from 230 ± 14 nm/s (for microtubule tips not coupled to beads and in the absence of force) to 44 ± 7 nm/s by beads coated with Ndc80 complex under 2 pN of force (Fig. 3*C*). For episodes of disassembly-driven movement against the applied force, about half (53 ± 8%) ended in bead detachment, but a large proportion (40 ± 7%) underwent a microtubule rescue (the remaining events, 7 ± 3%, terminated for other reasons, such as the bead reaching the microtubule seed or nonspecifically adhering to the cover-slip). Strikingly, disassembling microtubule tips coupled to beads coated with the Ndc80 complex rescued ~70-fold more frequently than bare microtubules (Fig. 3*D*) (135 ± 24 h^{-1} compared with 2 ± 1 h^{-1}). Therefore, the Ndc80 complex is an effective tip-coupler that can directly slow microtubule disassembly and promote rescue.

In contrast, in our previous work with the budding yeast Ndc80 complex, we observed little effect on the rate of microtubule rescue (23). Here we analyzed the dataset reported in Powers et al. (23), specifically looking for rescue events. Microtubules rescued at a frequency of 9 ± 5 h^{-1} while coupled to beads coated with budding yeast Ndc80 complex (n = 4 rescues, ~100–2,700 complexes per bead, against ~1 pN of force). This number is close to the rate of rescue for microtubules not coupled to beads (reported above). Therefore, the budding yeast Ndc80 complex, unlike the human complex, appears to have little ability to promote microtubule rescue.

Phosphomimetic Mutations in the Ndc80 Complex Inhibit Its Ability to Influence Microtubule Dynamics. The Hec1 protein of the Ndc80 complex contains a calponin homology domain that is important for its microtubule binding activity (29, 30). In addition, Hec1 has a disordered N-terminal tail that contributes to the affinity of

the complex for microtubules (11, 12, 30). In vivo, the tail is a target for the Aurora B kinase, and mutations that mimic phosphorylation at these sites result in unattached kinetochores (11, 43). Consistent with this observation, Aurora B phosphorylation of a truncated Ndc80 complex reduces its binding to microtubules in vitro (29). On the other hand, mutations that block phosphorylation severely damp kinetochore oscillations in vivo (8). These findings suggest that phosphorylation in the Hec1 tail is required not only for regulation of kinetochore-microtubule attachments, but also for normal kinetochore-microtubule dynamics. Using the optical trap assay, we tested the direct contribution of the tail to microtubule dynamics in vitro. In addition to the wild-type complex, we purified Ndc80 complex with the nine putative Aurora B target sites in the Hec1 tail mutated to aspartic acid to mimic phosphorylation (9D), and Ndc80 complex with the Hec1 tail deleted (ΔN). As a control, we also purified Ndc80 complex with alanine mutations at the Aurora B target sites (9A). Because this construct behaved like the wild-type complex in our TIRF assays (Figs. S3*B* and S4), it was not further characterized in the optical trap assay.

Beads coated with wild-type, 9D, and ΔN complexes were all able to slow the rate of microtubule disassembly in a concentration-dependent manner when tracking with disassembling tips against ~2 pN of applied force (Fig. 3 *B* and *C*). However, the 9D and ΔN complexes were impaired relative to the wild-type complex; when incubated with 5 nM of Ndc80 complex, 82 ± 11% of wild-type beads tracked with disassembling microtubule tips, but only 21 ± 5% of the 9D beads and 20 ± 4% of the ΔN beads tracked with disassembly (Fig. 3*B*). Furthermore, 5 nM wild-type beads slowed disassembly to 44 ± 7 nm/s, but 5 nM 9D and 5 nM ΔN beads slowed disassembly to 110 ± 20 and 96 ± 27 nm/s, respectively (Fig. 3*C*). The ability of the mutant complexes to track with and slow disassembly was recovered to wild-type levels by increasing the density of decoration on beads ~20-fold (Fig. 3 *B* and *C*: compare 0.5 and 1 nM wild-type to 10 and 20 nM mutant complexes, respectively). For example, beads coated with 20 nM 9D or 20 nM ΔN complex tracked with microtubules similarly to 1 nM wild-type beads (9D: 76 ± 11%; ΔN: 70 ± 10%; wild-type: 74 ± 9%). Therefore, increasing the number of mutant complexes on beads compensates for their decreased coupling performance.

When assayed at comparable coupling performance, the wild-type and ΔN complexes promoted microtubule rescue, but the 9D complex did not (Fig. 3 *D* and *E*). Deletion of the Hec1 tail reduced the ability of the complex to promote rescue only modestly (~twofold). In contrast, phosphomimetic mutations in the tail nearly abolished this activity. Using beads coated with 20 nM 9D complex, we observed only three rescue events in 29 min
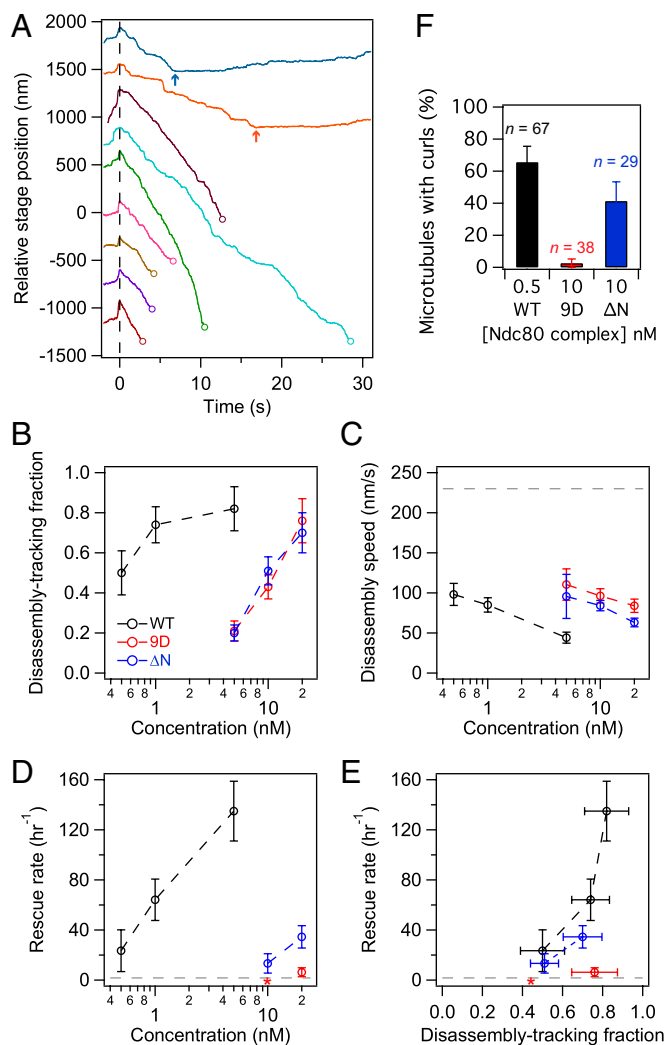
Fig. 3. Phosphomimetic mutations in the Ndc80 complex inhibit its ability to promote microtubule rescue. (*A*) Example traces of position vs. time for beads decorated with Ndc80 complex as they tracked microtubule disassembly against ~2 pN of applied force. Time $t = 0$ s (dashed vertical line) marks the onset of tracking, when the disassembling microtubule tip began to drive movement of the bead against the force of the trap. Disassembly-driven movement ended when the bead detached (open circles) or when the microtubule rescued (arrows). Traces are offset vertically for visual clarity. (*B*) The fraction of beads coated with wild-type or mutant Ndc80 complex capable of tracking against ~2 pN. From the disassembly-tracking events in *B*, (*C*) mean microtubule disassembly speeds ± SEM and (*D*) rescue rates were measured. Without load and in the absence of bead-bound Ndc80 complex, the disassembly rate was 230 ± 14 nm/s (dashed line in *C*, *n* = 26) and the rescue rate was 2 ± 1 h⁻¹ (dashed line in *D*, *n* = 3 events in 104 min of disassembly). (*E*) Rescue rate is plotted against the fraction of beads that tracked disassembly against force. (*F*) Percentage of microtubules for which a curl (Fig. 2*D* and Fig. S3*B*) was observed at either tip during disassembly in the TIRF microscopy assay. The *n* for each data point in *B–D* is listed in Table S1. Asterisks indicate that no rescues were observed. Unless otherwise noted, all error bars represent uncertainties from counting statistics.

of microtubule disassembly, which is an average rescue frequency similar to that for bare microtubules (6 ± 4 vs. 2 ± 1 h⁻¹). In addition, the ΔN complex but not the 9D complex stabilized curled extensions at disassembling microtubule tips in the TIRF assay (Fig. 3*F*). Thus, phosphomimetic mutations do not simply negate the activity of the tail, but actively interfere with the ability to modify microtubule tip structure and promote rescue.

The ΔN and 9D complexes performed similarly in tracking with and slowing microtubule disassembly, suggesting that their disparate effects on microtubule rescue and tip structure are not simply the result of a difference in their microtubule-binding affinities. We quantified binding of GFP-tagged 9D and ΔN complexes directly by single-molecule TIRF microscopy and bulk microtubule binding assays. Unlike the wild-type complex, binding of the mutant complexes was undetectable in standard BRB80 (120 mM K⁺) buffer conditions, so the assays were performed in BRB40 (60 mM K⁺) buffer. Single molecules of 9D and ΔN complex exhibited similar dissociation and diffusion rate constants (Fig. 4 *A* and *B*) ($k_{off} = 0.85 \pm 0.07$ and 0.90 ± 0.05 s⁻¹, and $D = 0.060 \pm 0.003$ and 0.050 ± 0.002 μm²·s⁻¹, respectively). In contrast, wild-type Ndc80 complexes dissociated from microtubules ~15-times more slowly ($k_{off} = 0.062 \pm 0.005$ s⁻¹) and diffused on the lattice ~four-times more slowly ($D = 0.015 \pm 0.001$ μm²·s⁻¹). It has been previously suggested that the Hec1 tail contributes to microtubule binding by the Ndc80 complex or mediates cooperativity between complexes on microtubules (11, 12, 28). Our results establish that the tail contributes directly to microtubule binding, because deletion of the tail causes individual Ndc80 complexes (in the absence of cooperative binding) to dissociate more quickly from microtubules.

In the bulk binding assay, fits to both the Hill and the McGhee and von Hippel models (Fig. 4 *C* and *D*) show that the 9D and ΔN complexes are indistinguishable from one another in their apparent affinities, cooperativity constants, and lattice occupancies (McGhee and von Hippel fit for 9D and ΔN: $K_d = 78 \pm 20$ and 73 ± 20 nM, $w = 7 \pm 2$ and 7 ± 1, $i = 2.4 \pm 0.1$ and 2.4 ± 0.1 per tubulin dimer, respectively). Therefore, phosphomimetic mutations reduce the affinity of the Ndc80 complex for microtubules and impair its ability to promote microtubule rescue. However, these two effects are not strictly coupled; deletion of the Hec1 tail equally reduces the affinity of the complex for microtubules, but is not as detrimental to its ability to modify microtubule tip structure and dynamics. These findings suggest that Aurora B phosphorylation has separable effects on attachment stability and microtubule dynamics at the kinetochore.

Discussion

Ndc80 Complex Directly Modulates Microtubule Dynamics. The Ndc80 complex is a conserved and essential microtubule-binding component of the kinetochore. Here, we characterized the binding of full-length human Ndc80 complex to microtubules in vitro. The Ndc80 complex bound cooperatively to microtubules with a strong affinity, and directly promoted microtubule rescue. Our in vitro results using unphosphorylated wild-type Ndc80 complex explain observations made in cells. In the absence of Hec1 phosphorylation, we found that the Ndc80 complex antagonizes microtubule disassembly. This effect explains why blocking Hec1 phosphorylation in vivo causes hyper-stabilized K-fibers, and leads to damped sister kinetochore oscillations and severe defects in cell division (8). We believe our findings are unique in representing a demonstration that a core component of the human kinetochore directly modifies microtubule rescue rate in vitro. This ability has been shown previously for a core kinetochore component only once, with the budding yeast Dam1 complex (44), which has no known homolog in higher eukaryotes. Notably, the budding yeast Ndc80 complex does not effectively promote microtubule rescue (23), even though the composition and domain structure of the complex are highly conserved.

Our results also indicate a possible mechanism by which the Ndc80 complex promotes microtubule rescue. In the absence of stabilizing factors, protofilaments at disassembling microtubule tips form tight ~20-nm curls (37). When microtubules are stabilized by a nonhydrolyzable GTP analog, protofilaments are straighter at disassembling tips (45). We found that the tips of disassembling microtubules in the presence of Ndc80 complex were gently
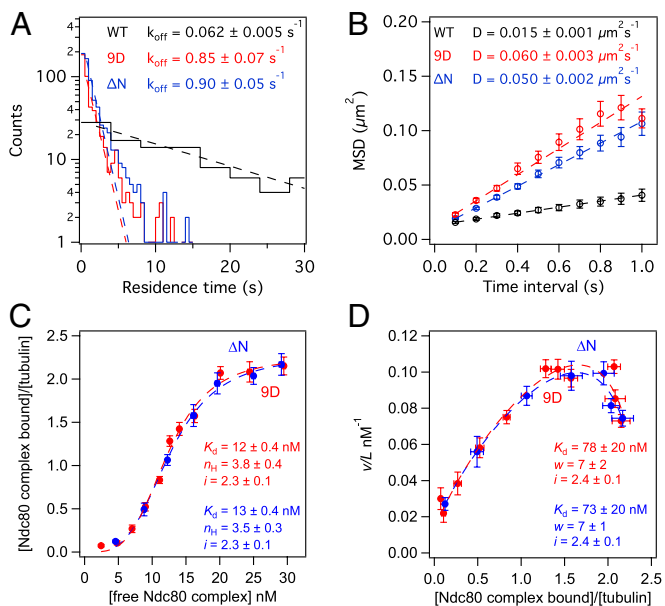
Fig. 4. The 9D and ΔN Ndc80 complexes exhibit similar binding behavior on microtubules. (*A*) Histograms of the residence time for single molecules (5 pM complex in solution) of wild-type (black trace, $n = 131$), 9D (red trace, $n = 497$), and ΔN (blue trace, $n = 705$) Ndc80 complex on taxol-stabilized microtubules. Each histogram was fit by a single exponential (dashed lines) to determine the off-rate constant, k_{off}. (*B*) Plots of MSD vs. time lag for binding events in *A*. The diffusion constant, *D*, was measured from linear fits to the data (dashed lines). (*C* and *D*) Bulk binding assays of 9D (red traces, $n = 4$–7 replicates per data point) and ΔN (blue traces, $n = 6$–7 replicates per data point) Ndc80 complex on taxol-stabilized microtubules. Dashed lines show fits of binding data to (*C*) Hill and (*D*) McGhee and von Hippel models. Errors on model fit parameters (K_d, n_H, w, and i) represent SD. All markers represent mean ± SEM and all assays were performed in BRB40 buffer (see [SI Materials and Methods](#)).

curved (as seen by TIRF microscopy) and formed large protofilament sheets (as seen by EM). These observations suggest that the Ndc80 complex promotes microtubule rescue by stabilizing tip structures with straighter protofilaments. Alushin et al. proposed that the Hec1 calponin homology domain recognizes the interface between tubulin monomers (28) at a putative hinge region (46). Our findings are consistent with this model. Ndc80 complex lacking the Hec1 tail was able to modify microtubule tip structure and promote rescue, indicating that other parts of the complex (outside of the tail) are primarily responsible for this activity. We propose that binding of the Hec1 calponin homology domain at the hinge region between tubulin subunits induces a straighter protofilament conformation that facilitates microtubule rescue.

Aurora B Regulates Microtubule Dynamics Through the Ndc80 Complex.

The Aurora B kinase has an established role in releasing aberrant kinetochore-microtubule attachments (1). Consistent with this model, PtK cells carrying a phosphomimetic mutant Ndc80 (9D) complex have unattached kinetochores (11, 43). We found that the human 9D complex bound to microtubules more weakly relative to the wild-type complex, as determined by three independent in vitro assays. (*i*) Single molecules of the 9D complex dissociated more quickly (>10-fold) from the microtubule lattice. (*ii*) In our bulk assays, binding of the 9D complex was undetectable under conditions in which the wild-type complex bound strongly to microtubules. (*iii*) At equal surface density on beads, the 9D complex was impaired in its ability to track with microtubule disassembly against force. In all three of these assays, the 9D complex behaved similarly to and not worse than Ndc80 complex that lacks the tail domain (ΔN). Therefore, mutations that mimic

complete phosphorylation of the Hec1 tail prevent the tail from contributing to microtubule binding.

In vivo observations suggest that in higher eukaryotes, Aurora B does not simply trigger kinetochore-microtubule detachment but additionally regulates microtubule dynamics (8, 10, 47). In PtK cells, syntelic kinetochore-microtubule attachments are not lost immediately following Aurora B activation (10). Instead, reactivation of Aurora B appears to induce disassembly of the kinetochore microtubules, and the kinetochores track with disassembly back to the centrosome, where the attachments are corrected. Our results offer insight into these observations. At higher surface densities on beads (20 nM), the 9D complex tracked robustly with disassembling microtubule tips against force. Based on geometric constraints (23), we estimate ∼80 complexes can interact with the microtubule tip at this surface density. This number is more than the number of Ndc80 complexes per microtubule in vivo (∼20 per microtubule), but fewer than the number of complexes at a single mammalian kinetochore, which binds 20–25 microtubules through more than 400 attachments (40, 48). Relative to the wild-type complex, the 9D and ΔN complexes are similarly impaired in their binding affinity and tracking performance. However, the ΔN complex promotes microtubule rescue, but the 9D complex does not. Thus, a phosphomimetic Hec1 tail interferes with the ability of the Ndc80 complex to modulate microtubule dynamics, possibly by blocking the ability of the calponin homology domain to stabilize a straighter protofilament conformation. Taken together, these in vitro observations explain how phosphorylation relieves microtubule stabilization at syntelic kinetochores to promote K-fiber disassembly, allowing the attached kinetochores to track back to the centrosome.

Here, we show that a conserved core microtubule-binding component of the human kinetochore directly influences microtubule dynamics. In addition, we find that phosphomimetic mutations of essential Aurora B phosphorylation sites in Hec1 not only weaken attachment, but also nearly abolish the ability of the Ndc80 complex to influence dynamics. These effects are separable, and might be independently tunable through phosphorylation of different subsets of target sites in the Hec1 tail. Taken together, our results indicate that microtubule dynamics can be regulated through Aurora B phosphorylation of the Ndc80 complex.

Materials and Methods

Protein Expression and Purification. The Ndc80 complex was coexpressed from two di-cistronic plasmids encoding Spc25/Spc24-His6 and Hec1/Nuf2 (see [SI Materials and Methods](#)) in *E. coli* BL21 cells (Rosetta; Novagen). Protein expression and purification were carried out as previously described (23).

TIRF Microscopy. TIRF microscopy was performed on a custom illumination system (49) (see [SI Materials and Methods](#)). Taxol-stabilized Alexa-647-labeled microtubules were bound to the cover-slip with "rigor" kinesin (50). GFP-tagged Ndc80 complex was assayed in BRB80 (80 mM Pipes, 120 mM K⁺, 1 mM MgCl₂, and 1 mM EGTA, pH 6.9) or BRB40 (40 mM Pipes, 60 mM K⁺, 1 mM MgCl₂, and 1 mM EGTA, pH 6.9) with 8 mg·mL⁻¹ BSA, 10 μM taxol, and an oxygen scavenger system. For dynamic microtubule assays, GMPCPP-stabilized microtubule seeds were bound to the cover-slip using "rigor" kinesin, and Alexa-647-labeled extensions were grown in BRB80 containing 8 mg·mL⁻¹ BSA and 1 mM GTP. Microtubule disassembly was triggered by buffer exchange to remove free tubulin and simultaneously introduce GFP-tagged Ndc80 complex in BRB80 with 8 mg·mL⁻¹ BSA, 1 mM GTP, and an oxygen scavenger system. See [SI Materials and Methods](#) for additional details.

Microtubule Binding Assays. Microtubule binding assays were performed as previously described (32), with the following modifications: GFP-tagged Ndc80 complex was incubated with taxol-stabilized microtubules in BRB80 with 10 μM taxol and 8% (vol/vol) gel filtration buffer (50 mM Hepes, 200 mM NaCl, pH 7.6), and pelleted through a glycerol cushion onto a cover-slip. The amount of microtubule-bound Ndc80 complex was quantified by fluorescence microscopy. Increasing concentrations of the complex (0–15 nM) were assayed with microtubules (2.5 nM tubulin dimers) to generate a binding curve. Microtubule binding for the 9D and ΔN Ndc80 complexes was undetectable in

BRB80, so binding assays were performed with 0–35 nM complex in BRB40. Binding curves were fitted to the Hill (34) and McGhee and von Hippel (35) models in Igor Pro (Wavemetrics) using iterative least-squares fitting. Errors on curve fit parameters (K_d, n_H, w, and i) represent the SD estimated by Igor Pro. See *SI Materials and Methods* for details of the assay.

Electron Microscopy. Ndc80 complex (50 nM) was incubated with taxol-stabilized microtubules (37 nM tubulin dimers) in BRB80 with 10 μM taxol. For disassembly assays, microtubules were assembled in the absence of taxol and disassembly was induced by dilution into BRB80 containing 25 nM Ndc80 complex. Samples were applied onto carbon-coated copper grids and stained with uranyl formate. Grids were viewed on a transmission electron microscope (Spirit T12; FEI). Additional details are provided in *SI Materials and Methods*.

Optical Trap Bead Motility Assays. Anti-His$_5$ antibody-coated polystyrene beads (11 pM) were functionalized by incubation with His$_6$-tagged wild-type (0.5–5 nM) or mutant (5–20 nM) Ndc80 complex. Beads were attached to the tips of disassembling microtubule extensions, which were grown from GMPCPP-stabilized microtubule seeds bound to the cover-slip. An optical trap was used to apply a constant force of ~2 pN opposite the direction of microtubule disassembly. Assays were performed in BRB80 containing 1.4 mg·mL^{-1} tubulin, 8 mg·mL^{-1} BSA, 1 mM DTT, 250 μg·mL^{-1} glucose oxidase, 30 μg·mL^{-1} catalase, and 4.5 μg·mL^{-1} glucose. Records of bead position over time were generated and analyzed using custom software (Labview and Igor Pro, respectively). These data were used to determine the fraction of beads that tracked with disassembly, and the rates of microtubule disassembly and rescue. Additional details are included in *SI Materials and Methods*.

1. Liu D, Lampson MA (2009) Regulation of kinetochore-microtubule attachments by Aurora B kinase. *Biochem Soc Trans* 37:976–980.
2. Biggins S, Murray AW (2001) The budding yeast protein kinase Ipl1/Aurora allows the absence of tension to activate the spindle checkpoint. *Genes Dev* 15:3118–3129.
3. Cheeseman IM, et al. (2002) Phospho-regulation of kinetochore-microtubule attachments by the Aurora kinase Ipl1p. *Cell* 111:163–172.
4. Hauf S, et al. (2003) The small molecule Hesperadin reveals a role for Aurora B in correcting kinetochore-microtubule attachment and in maintaining the spindle assembly checkpoint. *J Cell Biol* 161:281–294.
5. Pinsky BA, Kung C, Shokat KM, Biggins S (2006) The Ipl1-Aurora protein kinase activates the spindle checkpoint by creating unattached kinetochores. *Nat Cell Biol* 8:78–83.
6. Tanaka TU, et al. (2002) Evidence that the Ipl1-Sli15 (Aurora kinase-INCENP) complex promotes chromosome bi-orientation by altering kinetochore-spindle pole connections. *Cell* 108:317–329.
7. Cimini D, Wan X, Hirel CB, Salmon ED (2006) Aurora kinase promotes turnover of kinetochore microtubules to reduce chromosome segregation errors. *Curr Biol* 16:1711–1718.
8. DeLuca KF, Lens SM, DeLuca JG (2011) Temporal changes in Hec1 phosphorylation control kinetochore-microtubule attachment stability during mitosis. *J Cell Sci* 124:622–634.
9. Cimini D, Moree B, Canman JC, Salmon ED (2003) Merotelic kinetochore orientation occurs frequently during early mitosis in mammalian tissue cells and error correction is achieved by two different mechanisms. *J Cell Sci* 116:4213–4225.
10. Lampson MA, Renduchitala K, Khodjakov A, Kapoor TM (2004) Correcting improper chromosome-spindle attachments during cell division. *Nat Cell Biol* 6:232–237.
11. Guimaraes GJ, Dong Y, McEwen BF, Deluca JG (2008) Kinetochore-microtubule attachment relies on the disordered N-terminal tail domain of Hec1. *Curr Biol* 18:1778–1784.
12. Miller SA, Johnson ML, Stukenberg PT (2008) Kinetochore attachments require an interaction between unstructured tails on microtubules and Ndc80(Hec1). *Curr Biol* 18:1785–1791.
13. Hunter AW, et al. (2003) The kinesin-related protein MCAK is a microtubule depolymerase that forms an ATP-hydrolyzing complex at microtubule ends. *Mol Cell* 11:445–457.
14. Jiang K, et al. (2009) TIP150 interacts with and targets MCAK at the microtubule plus ends. *EMBO Rep* 10:857–865.
15. Knowlton AL, Lan W, Stukenberg PT (2006) Aurora B is enriched at merotelic attachment sites, where it regulates MCAK. *Curr Biol* 16:1705–1710.
16. Manna T, Honnappa S, Steinmetz MO, Wilson L (2008) Suppression of microtubule dynamic instability by the +TIP protein EB1 and its modulation by the CAP-Gly domain of p150glued. *Biochemistry* 47:779–786.
17. Tirnauer JS, Grego S, Salmon ED, Mitchison TJ (2002) EB1-microtubule interactions in *Xenopus* egg extracts: Role of EB1 in microtubule stabilization and mechanisms of targeting to microtubules. *Mol Biol Cell* 13:3614–3626.
18. Zhang X, Lan W, Ems-McClung SC, Stukenberg PT, Walczak CE (2007) Aurora B phosphorylates multiple sites on mitotic centromere-associated kinesin to spatially and temporally regulate its function. *Mol Biol Cell* 18:3264–3276.
19. Zimniak T, Stengl K, Mechtler K, Westermann S (2009) Phosphoregulation of the budding yeast EB1 homologue Bim1p by Aurora/Ipl1p. *J Cell Biol* 186:379–391.
20. Kline-Smith SL, Sandall S, Desai A (2005) Kinetochore-spindle microtubule interactions during mitosis. *Curr Opin Cell Biol* 17:35–46.
21. Wei RR, et al. (2006) Structure of a central component of the yeast kinetochore: The Spc24p/Spc25p globular domain. *Structure* 14:1003–1009.
22. Wei RR, Sorger PK, Harrison SC (2005) Molecular organization of the Ndc80 complex, an essential kinetochore component. *Proc Natl Acad Sci USA* 102:5363–5367.
23. Powers AF, et al. (2009) The Ndc80 kinetochore complex forms load-bearing attachments to dynamic microtubule tips via biased diffusion. *Cell* 136:865–875.
24. Tien JF, et al. (2010) Cooperation of the Dam1 and Ndc80 kinetochore complexes enhances microtubule coupling and is regulated by aurora B. *J Cell Biol* 189:713–723.
25. Lampert F, Hornung P, Westermann S (2010) The Dam1 complex confers microtubule plus end-tracking activity to the Ndc80 kinetochore complex. *J Cell Biol* 189:641–649.
26. Cheeseman IM, Chappie JS, Wilson-Kubalek EM, Desai A (2006) The conserved KMN network constitutes the core microtubule-binding site of the kinetochore. *Cell* 127:983–997.
27. Tooley JG, Miller SA, Stukenberg PT (2011) The Ndc80 complex uses a tripartite attachment point to couple microtubule depolymerization to chromosome movement. *Mol Biol Cell* 22:1217–1226.
28. Alushin GM, et al. (2010) The Ndc80 kinetochore complex forms oligomeric arrays along microtubules. *Nature* 467:805–810.
29. Ciferri C, et al. (2008) Implications for kinetochore-microtubule attachment from the structure of an engineered Ndc80 complex. *Cell* 133:427–439.
30. Wei RR, Al-Bassam J, Harrison SC (2007) The Ndc80/HEC1 complex is a contact point for kinetochore-microtubule attachment. *Nat Struct Mol Biol* 14:54–59.
31. Wilson-Kubalek EM, Cheeseman IM, Yoshioka C, Desai A, Milligan RA (2008) Orientation and structure of the Ndc80 complex on the microtubule lattice. *J Cell Biol* 182:1055–1061.
32. Graczyk B, Davis TN (2011) An assay to measure the affinity of proteins for microtubules by quantitative fluorescent microscopy. *Anal Biochem* 410:313–315.
33. Gestaut DR, et al. (2008) Phosphoregulation and depolymerization-driven movement of the Dam1 complex do not require ring formation. *Nat Cell Biol* 10:407–414.
34. Hill AV (1910) The possible effects of the aggregation of molecules of haemoglobin on its dissociation curves. *J Physiol* 40:iv–vii.
35. McGhee JD, von Hippel PH (1974) Theoretical aspects of DNA-protein interactions: Co-operative and non-co-operative binding of large ligands to a one-dimensional homogeneous lattice. *J Mol Biol* 86:469–489.
36. Koshland DE, Mitchison TJ, Kirschner MW (1988) Polewards chromosome movement driven by microtubule depolymerization in vitro. *Nature* 331:499–504.
37. Mandelkow EM, Mandelkow E, Milligan RA (1991) Microtubule dynamics and microtubule caps: A time-resolved cryo-electron microscopy study. *J Cell Biol* 114:977–991.
38. Westermann S, et al. (2005) Formation of a dynamic kinetochore- microtubule interface through assembly of the Dam1 ring complex. *Mol Biol Cell* 17:277–290.
39. Franck AD, Powers AF, Gestaut DR, Davis TN, Asbury CL (2010) Direct physical study of kinetochore-microtubule interactions by reconstitution and interrogation with an optical force clamp. *Methods* 51:242–250.
40. Lawrimore J, Bloom KS, Salmon ED (2011) Point centromeres contain more than a single centromere-specific Cse4 (CENP-A) nucleosome. *J Cell Biol* 195:573–582.
41. Nicklas RB (1988) The forces that move chromosomes in mitosis. *Annu Rev Biophys Biophys Chem* 17:431–449.
42. Pearson CG, Maddox PS, Salmon ED, Bloom K (2001) Budding yeast chromosome structure and dynamics during mitosis. *J Cell Biol* 152:1255–1266.
43. Sundin LJ, Guimaraes GJ, Deluca JG (2011) The NDC80 complex proteins Nuf2 and Hec1 make distinct contributions to kinetochore-microtubule attachment in mitosis. *Mol Biol Cell* 22:759–768.
44. Franck AD, et al. (2007) Tension applied through the Dam1 complex promotes microtubule elongation providing a direct mechanism for length control in mitosis. *Nat Cell Biol* 9:832–837.
45. Müller-Reichert T, Chrétien D, Severin F, Hyman AA (1998) Structural changes at microtubule ends accompanying GTP hydrolysis: Information from a slowly hydrolyzable analogue of GTP, guanylyl (alpha,beta)methylenediphosphonate. *Proc Natl Acad Sci USA* 95:3661–3666.
46. Wang HW, Nogales E (2005) Nucleotide-dependent bending flexibility of tubulin regulates microtubule assembly. *Nature* 435:911–915.
47. DeLuca JG, et al. (2006) Kinetochore microtubule dynamics and attachment stability are regulated by Hec1. *Cell* 127:969–982.
48. Rieder CL (1982) The formation, structure, and composition of the mammalian kinetochore and kinetochore fiber. *Int Rev Cytol* 79:1–58.
49. Gestaut DR, Cooper J, Asbury CL, Davis TN, Wordeman L (2010) Reconstitution and functional analysis of kinetochore subcomplexes. *Methods Cell Biol* 95:641–656.
50. Rice S, et al. (1999) A structural change in the kinesin motor protein that drives motility. *Nature* 402:778–784.

Supporting Information

Umbreit et al. 10.1073/pnas.1209615109

SI Materials and Methods

Cloning. The human Ndc80 complex was coexpressed in *Escherichia coli* from two di-cistronic plasmids: one encoded Spc25 and His$_6$-tagged Spc24 in the pCDF backbone, and the other encoded Hec1 and Nuf2 in the pST39 backbone. To generate the Spc25/Spc24-His$_6$ plasmid, cDNA clones of Spc25 and Spc24 were purchased from ATCC and cloned into pST39 (1) using XbaI/ApaI and EcoRI/HindIII, respectively. A C-terminal His$_6$-tag was added to Spc24 for affinity purification and binding to polystyrene beads. The di-cistron of Spc25/Spc24-His$_6$ was transferred from the pST39 backbone into the pCDF backbone (Merck KGaA) using AscI (added by PCR amplification). To generate the Hec1/Nuf2 plasmid, cDNA clones of Hec1 (purchased from ATCC) and Nuf2 (kindly provided by Jennifer DeLuca, Colorado State University, Fort Collins, CO) were inserted into pST39 using EcoRV/KpnI and BspEI/MluI, respectively. For GFP-tagged Ndc80 complex expression, three fragments were generated and ligated together to clone GFP onto the C terminus of human Nuf2. First, the C terminus of Nuf2 was removed from the Hec1/Nuf2 pST39 plasmid using SphI and MluI. Second, a Nuf2 fragment was created by PCR to introduce a PacI site in place of the stop codon, and cut with SphI/PacI. Third, a GFP fragment was similarly created by PCR, to introduce sites for and cut with PacI and MluI. Simultaneous ligation of all three fragments generated pST39 containing a di-cistron of Hec1 and Nuf2-GFP. Ndc80 complex mutants were generated by site-directed mutagenesis using QuikChange Lightning kits (Stratagene) according to the manufacturer's protocol.

Total Internal Reflection Fluorescence Microscopy. Total internal reflection fluorescence (TIRF) microscopy was performed as previously described (2–5). A far-red laser (FTEC-635-0-25-PFQ; Blue Sky Research) and blue laser (Sapphire 488-75; Coherent) were used for simultaneous excitation of Alexa-647 and GFP. The illumination light reaching the sample was collimated and collected through the objective lens (CFI Planapochromat, 100×, 1.49 numerical aperture; Nikon). Emission channels from GFP and Alexa-647 were projected side-by-side onto a CCD camera (iXon 887-BI; Andor Technology), and images were collected at 10 frames per second with iXon software (Andor Technology).

Flow cells for TIRF microscopy were constructed and prepared as previously described (3). Flow cells were washed with H$_2$O and subsequently incubated for 5 min with "rigor" kinesin (6) diluted in BRB80 (80 mM Pipes, 120 mM K$^+$, 1 mM MgCl$_2$, and 1 mM EGTA, pH 6.9) with 8 mg·mL^{-1} BSA. Taxol-stabilized microtubules (1% Alexa-647–labeled tubulin) were bound for ~1 min and washed with BRB80 containing 8 mg·mL^{-1} BSA and 10 μM taxol. Flow cells were washed again with BRB80 or BRB40 (40 mM Pipes, 60 mM K$^+$, 1 mM MgCl$_2$, and 1 mM EGTA, pH 6.9) containing 8 mg·mL^{-1} BSA, 10 μM taxol, and an oxygen scavenger system (200 μg·mL^{-1} glucose oxidase, 35 μg·mL^{-1} catalase, 25 mM glucose and 5 mM DTT). GFP-tagged Ndc80 complex was introduced in BRB80 or BRB40 with 8 mg·mL^{-1} BSA, 10 μM taxol and an oxygen scavenger system. Single-molecule conditions were confirmed by measuring photobleach steps (at various excitation laser powers) for wild-type Ndc80 complexes on taxol-stabilized microtubules (Fig. S2). Laser powers were measured before entry into the microscope body.

In the dynamic microtubule TIRF experiments, GMPCPP-stabilized seeds (2% Alexa-647–labeled) were bound to the cover-slip with "rigor" kinesin and washed with growth buffer (BRB80 with 8 mg·mL^{-1} BSA and 1 mM GTP). Dynamic extensions were polymerized off the seeds by the addition of growth buffer supplemented with 2 mg·mL^{-1} tubulin (1% Alexa-647–labeled) and an oxygen scavenger system. Disassembly was induced by buffer exchange with BRB80 containing 8 mg·mL^{-1} BSA, an oxygen scavenger system, and the reported concentration of GFP-labeled Ndc80 complex. All dynamic microtubule assays were done at 30 °C.

Software analysis was performed using Labview (National Instruments), as previously described (2–5). Kymographs were generated for both the Alexa-647 and GFP channels. The position and brightness over time was recorded for individual GFP-tagged complexes on microtubules. Custom programs (available upon request) written in Igor Pro (Wavemetrics) were used to generate residence time histograms and standard diffusion rate plots (mean-squared displacement vs. time lag). The dissociation rate constant (k_{off}) was calculated from a single exponential fit to the histogram of residence time. Diffusion rate constants were calculated from linear fits to diffusion plots. For dynamic microtubule assays, disassembly rates were measured as the average distance disassembled over time, as determined from Alexa-647 channel kymographs. Disassembly rates were measured only for the longer extension of each microtubule, and extensions shorter than 4 μm were discarded from analysis because of unreliability in measurements for short events. Microtubule tips were scored visually for the formation of extensions that curled away from the long axis of the microtubule during disassembly (Fig. S3 *A* and *B*). Only microtubules for which the tip was in focus throughout disassembly were scored.

Microtubule Binding Assays. The bulk binding assay was performed as previously described (3, 7). GFP-tagged Ndc80 complex was incubated with Alexa-568-labeled taxol-stabilized microtubules (2.5 nM tubulin dimers) for 10 min at room temperature. The incubation was done in BRB80 or BRB40 with 10 μM taxol and 8% gel filtration buffer (50 mM Hepes, 200 mM NaCl, pH 7.6). The reaction was fixed by addition of three volumes of 2% glutaraldehyde in BRB80 or BRB40 and incubated for 2 min at room temperature. The assay is not sensitive to the amount of glutaraldehyde used or the duration of the fix (7). A 750-μL glycerol cushion (15% wt/vol in PBS) was layered on top of a polylysine-treated glass cover-slip sitting on a custom spacer (Ellard Instrumentation) in a TLS-55 centrifuge tube (Beckman). A 250-μL portion of the fixed reaction mixture was layered onto the glycerol cushion and the microtubules were pelleted onto the cover-slip at 135,000 × *g* for 10 min at 25 °C. The supernatant and glycerol cushion were removed by aspiration and the cover-slip was placed onto a drop of Citifluor (Ted Pella), microtubule-side down, on a glass slide. The slide was sealed with nail polish to prevent evaporation.

Slides were imaged on a DeltaVision microscopy system (Applied Precision) containing an Olympus IX70 microscope, a 100× oil objective (1.35 numerical aperture), and a CoolSnap HQ digital camera (Roper Scientific). For each slide, 10 *z*-sections (0.3 μm) were taken in 10 consecutive panels (512 × 512 pixels, binned 2 × 2) using filter sets to detect GFP and Alexa-568. To determine the amount of GFP-tagged Ndc80 complex for each slide, the average pixel intensity for the second *z*-section image in the GFP channel was averaged for the 10 panels. These values were corrected for background (a slide in which microtubules were incubated in the absence of Ndc80 complex) and lamp intensity (using the photosensor value). Standard curves were made by incubating increasing concentrations (up to ~60 nM) of wild-type or mutant

Ndc80 complex with a saturating amount of microtubules (140 nM) in the appropriate buffers (BRB80 or BRB40), such that all Ndc80 complex added to the reaction was bound to microtubules. Microtubules were pelleted and imaged as described above. Slopes from the standard curves were used to convert fluorescence intensity values to concentrations for microtubule-bound Ndc80 complexes.

Electron Microscopy. Taxol-stabilized microtubules (37 nM tubulin dimers) were incubated with wild-type Ndc80 complex (50 nM) in BRB80 containing 10 μM taxol for ~10 min. Copper grids were carbon-coated and positively charged in a glow discharge device (EMS) at 25 mA for 2 min. A drop of the reaction mix (2 μL) was applied onto a freshly discharged grid and incubated for 20 s. Excess sample was blotted off, the grid was washed twice with BRB80, once with 0.075% uranyl formate, and stained with uranyl formate. Excess stain was blotted off and the grid was air-dried. Grids were viewed on a transmission electron microscope (Spirit T12, FEI) operating at 120 kV and images were recorded on a 1 k × 1 k bottom-mount slow-scan CCD camera (Gatan) at a nominal magnification of 21,000× at the specimen level.

For the disassembly assay, microtubules were assembled by incubating cleared tubulin (~6 μg/μL) in BRB80 containing 2 mM GTP, 5 mM $MgCl_2$, and 4% DMSO at 37 °C for 30 min. After assembly, 1 volume of warm BRB80 (37 °C) was added to make the stock microtubule mix. Disassembly was induced by diluting 1 μL of microtubule mix into 200 μL of a filtered BRB80 solution (0.22-μm filter; Millipore) containing 25 nM human Ndc80 complex, 25 nM budding yeast Dam1 complex (8), or 10 μM taxol, and incubating for 2 min at room temperature. Samples were then prepared for analysis and imaged by electron microscopy, as described above.

Optical Trap Bead Motility Assays. Ndc80 complexes were linked to the surface of polystyrene beads, as previously described (4, 5, 9). Streptavidin-coated beads (Spherotech) were functionalized with biotinylated anti-His_5 antibodies (Qiagen). His_6-tagged wild-type or mutant Ndc80 complex was incubated at the appropriate concentration (0.5, 1, 5, 10, or 20 nM) with 11 pM beads, rotating for 30 min at 4 °C. Beads were spun down at $16,100 \times g$ in a desktop centrifuge for 5 min at 4 °C, and resuspended in 200 μL assay buffer (BRB80 containing 8 mg·mL^{-1} BSA and 1 mM DTT) to wash away unbound Ndc80 complex. The beads were spun again at $16,100 \times g$ for 5 min at 4 °C, and resuspended with assay buffer to the original incubation volume.

Flow chambers were constructed and functionalized as previously described (9). First, one flow chamber volume of 1 mg·mL^{-1} biotinylated BSA (Vector Laboratories) was introduced and allowed to bind to the glass surface for ~10 min at room temperature. The chamber was then washed twice with ~20 volumes BRB80. Next,

~10 volumes 0.33 mg·mL^{-1} avidin DN (Vector Laboratories) was introduced, incubated for ~2 min, and washed out with ~20 volumes BRB80. GMPCPP-stabilized biotinylated microtubule seeds were introduced in BRB80, and allowed to bind to the functionalized glass surface for ~2 min. The chamber was then washed with ~20 volumes blocking buffer (BRB80 containing 1 mM GTP, 8 mg·mL^{-1} BSA, and 1 mg·mL^{-1} κ-casein), followed by a second wash with growth buffer (BRB80 containing 1 mM GTP and 8 mg·mL^{-1} BSA). Lastly, Ndc80 complex-coated beads were introduced at an eightfold dilution from the incubation mix (see above) in a solution of growth buffer containing 1.4 mg·mL^{-1} tubulin, 8 mg·mL^{-1} BSA, 1 mM DTT, 250 μg·mL^{-1} glucose oxidase, 30 μg·mL^{-1} catalase, and 4.5 μg·mL^{-1} glucose. The edges of the flow chamber were sealed with nail polish to prevent evaporation. Microtubule disassembly events occurred either by a spontaneous switch from assembly to disassembly or by laser scission, as described previously (9). All optical trap assays were performed at 26 °C.

Records of bead position vs. time were analyzed using custom software written in Igor Pro (available upon request). To be considered in the analysis, beads were required to have undergone tracking in the direction of disassembly against the applied force for at least 25 nm. Detachments were scored during the experiment and verified in analysis when the force on a bead under load suddenly dropped to zero, and the bead position trace exhibited "run-away" movement. Microtubule rescues were scored visually during the experiment and verified in analysis by identifying the time at which microtubule disassembly halted. Beads were observed for an additional ~30 s to verify that the bead subsequently underwent motion in the direction of microtubule growth at an assembly-limited rate (~10 nm/s) (Fig. 3A, top two traces). Intrinsic disassembly and rescue rates for bare microtubules in the absence of force were measured from traces of tip position versus time, as determined from differential interference contrast recordings (10). We also determined that microtubule rescue was not a result of the disassembling tip reaching the GMPCPP-stabilized microtubule seed; the microtubule lattice was laser-ablated approximately at the point where rescue occurred, and the microtubule was verified to undergo disassembly back to the stabilized seed. The rescue rate for microtubules was calculated by dividing the number of observed microtubule rescues by the total time of disassembly-driven motility recorded for each assay condition. Disassembly rates were estimated for each event by the slope of a linear fit to the bead position versus time trace, taken over the second half of the entire duration of the disassembly event. Events that lasted less than 2 s were not included in disassembly rate analysis because of unreliability in the linear fits over short time intervals.

1. Tan S (2001) A modular polycistronic expression system for overexpressing protein complexes in *Escherichia coli*. *Protein Expr Purif* 21:224–234.
2. Gestaut DR, Cooper J, Asbury CL, Davis TN, Wordeman L (2010) Reconstitution and functional analysis of kinetochore subcomplexes. *Methods Cell Biol* 95:641–656.
3. Gestaut DR, et al. (2008) Phosphoregulation and depolymerization-driven movement of the Dam1 complex do not require ring formation. *Nat Cell Biol* 10:407–414.
4. Powers AF, et al. (2009) The Ndc80 kinetochore complex forms load-bearing attachments to dynamic microtubule tips via biased diffusion. *Cell* 136:865–875.
5. Tien JF, et al. (2010) Cooperation of the Dam1 and Ndc80 kinetochore complexes enhances microtubule coupling and is regulated by aurora B. *J Cell Biol* 189:713–723.
6. Rice S, et al. (1999) A structural change in the kinesin motor protein that drives motility. *Nature* 402:778–784.

7. Graczyk B, Davis TN (2011) An assay to measure the affinity of proteins for microtubules by quantitative fluorescent microscopy. *Anal Biochem* 410:313–315.
8. Franck AD, et al. (2007) Tension applied through the Dam1 complex promotes microtubule elongation providing a direct mechanism for length control in mitosis. *Nat Cell Biol* 9:832–837.
9. Franck AD, Powers AF, Gestaut DR, Davis TN, Asbury CL (2010) Direct physical study of kinetochore-microtubule interactions by reconstitution and interrogation with an optical force clamp. *Methods* 51:242–250.
10. Walker RA, et al. (1988) Dynamic instability of individual microtubules analyzed by video light microscopy: Rate constants and transition frequencies. *J Cell Biol* 107:1437–1448.
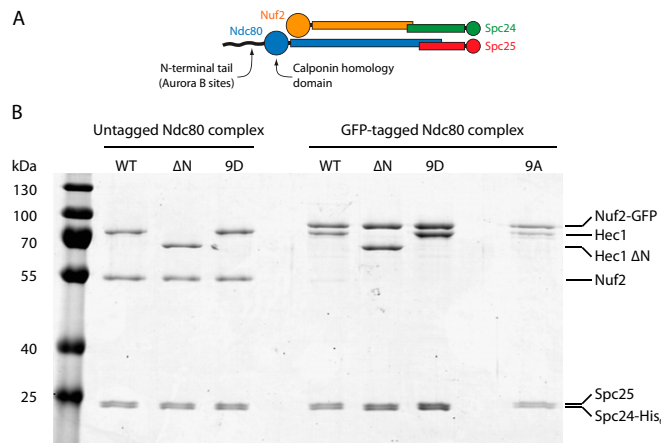
Fig. S1. The human Ndc80 complex was expressed in and purified from *E. coli* using affinity and size-exclusion chromatography. (*A*) Schematic of the heterotetrameric Ndc80 complex. (*B*) A Coomassie-stained gel shows the purified, recombinant wild-type and mutant versions of the Ndc80 complex used in this study. Molecular weight size markers are labeled on the left, and Ndc80 complex proteins, identified by size, are labeled on the right.
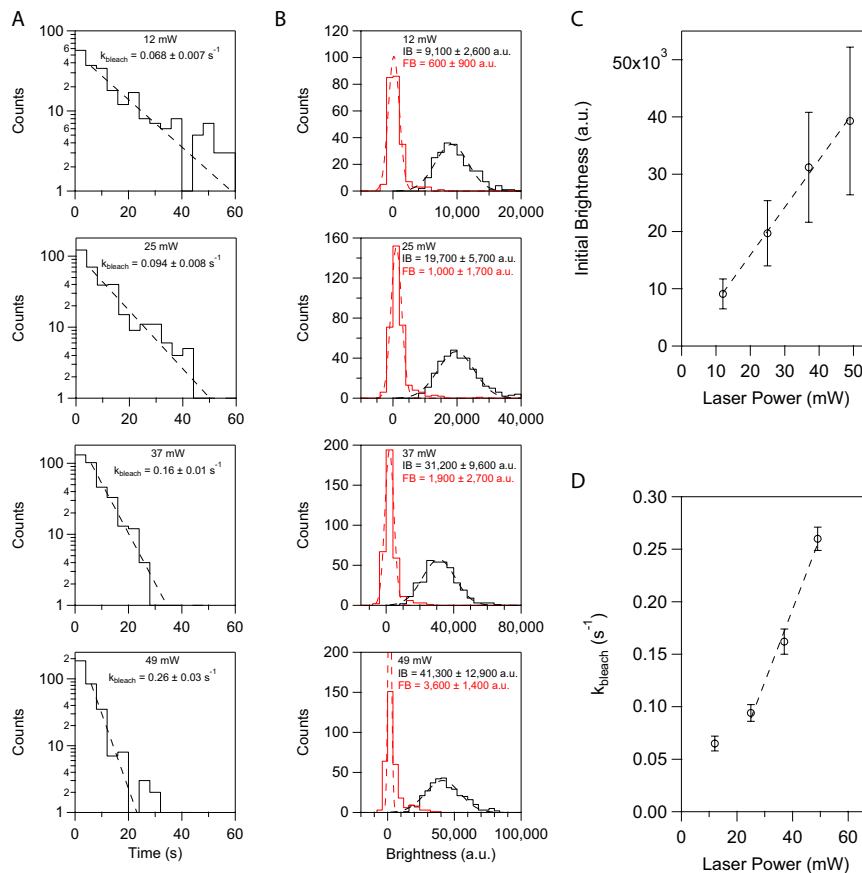

Fig. S2. The Ndc80 complex binds microtubules primarily as a monomer in the single-molecule TIRF assay. To determine if the GFP-tagged Ndc80 complex binds microtubules as a monomer in our single-molecule conditions (5–10 pM complex in solution), we imaged individual particles in BRB40 buffer under conditions that enhanced photobleaching. For example, a monomer would photobleach to near-background levels in a single step, whereas a dimer would photobleach in two steps of half the initial particle brightness. (*A*) Histograms of residence time with exponential fits (dashed lines) used to calculate the apparent bleach rate constant, k_{bleach} (a combination of GFP photobleaching rate and off-rate constants), at various excitation laser intensities. (*B*) Histograms and corresponding Gaussian fits of initial brightness (IB, black traces) and final brightness after photobleaching or detachment (FB, red traces). Note that the single bleach step (∼95% of IB) for each condition is consistent with a monomeric species. (*C*) Plot of initial brightness vs. laser power with a linear fit (dashed line). (*D*) Plot of k_{bleach} vs. laser power. Above 12 mW, k_{bleach} increases linearly with laser power (dashed line), indicating that photobleaching (rather than detachment) contributes primarily to k_{bleach} under these conditions. For the datasets in *A*–*D*: $n = 228$ at 12 mW, $n = 337$ at 25 mW, $n = 347$ at 37 mW, and $n = 327$ at 49 mW.
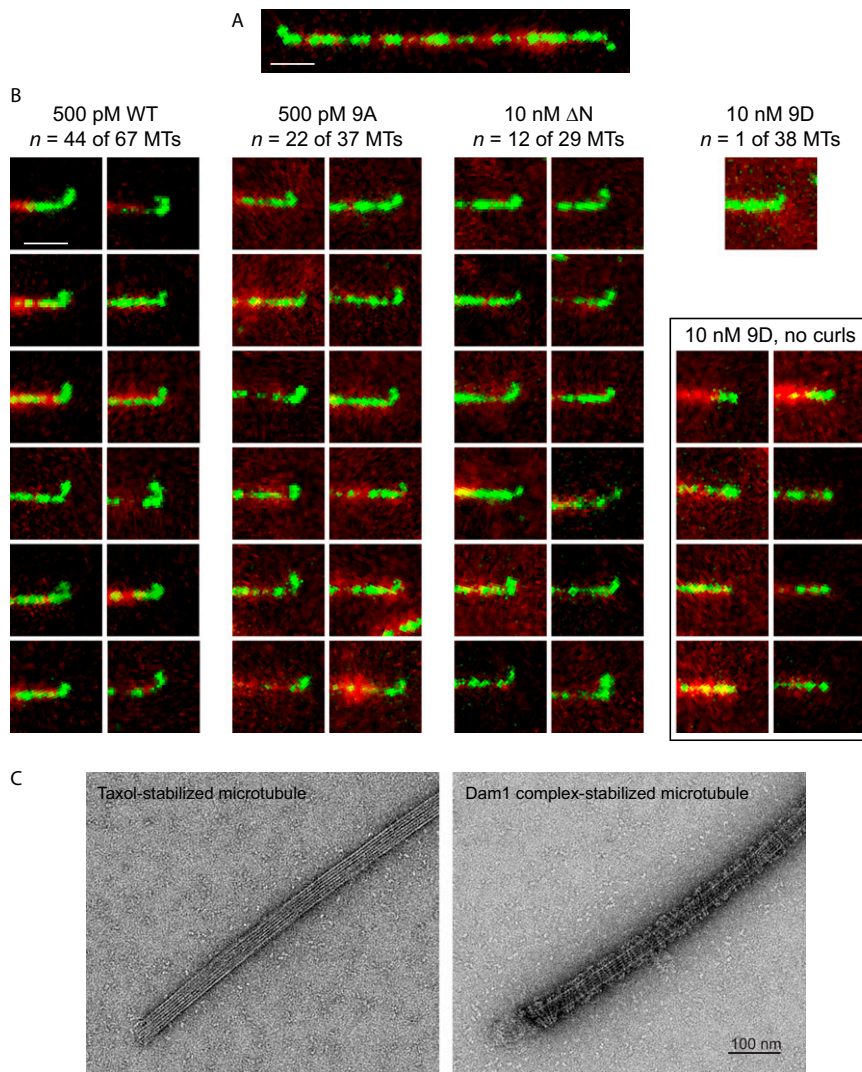
Fig. S3. Curls form at disassembling microtubule tips in the presence of Ndc80 complex. (*A*) In the presence of 500 pM GFP-tagged wild-type Ndc80 complex (green), curled extensions were observed at both ends of disassembling Alexa-647-labeled microtubules (red). (Scale bar, 2 μm.) (*B*) Gallery of curled extensions at the tips of disassembling microtubules in the presence of wild-type, 9A, ΔN, and 9D Ndc80 complex. The number (*n*) of microtubules (MTs) that formed curled extensions during disassembly is noted for each condition. (Scale bar, 2 μm.) (*C*) Negative-stain electron micrographs of disassembling microtubule tips (see *SI Materials and Methods*) stabilized by taxol or budding yeast Dam1 complex.
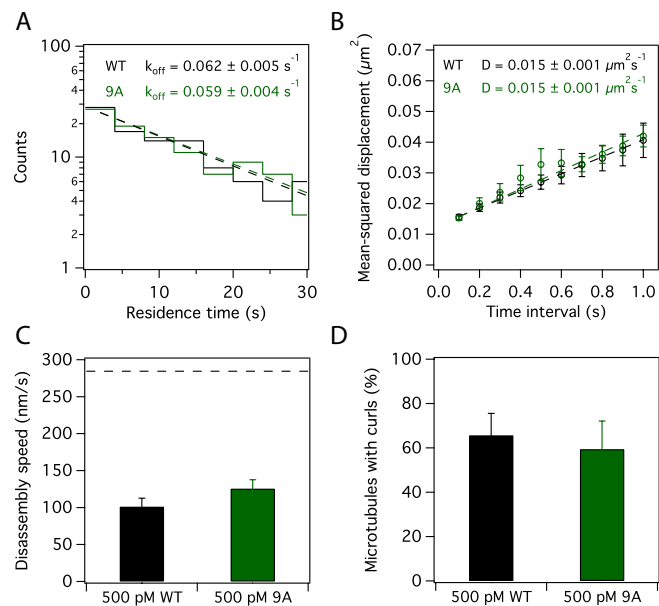
Fig. S4. Wild-type and 9A Ndc80 complexes exhibit similar binding behavior on microtubules. By TIRF microscopy, single molecules (5 pM complex in solution) of GFP-tagged wild-type (black traces, from Fig. 4 *A* and *B*) and 9A (green traces, *n* = 124) Ndc80 complexes have similar (*A*) residence time distributions and (*B*) diffusion rates on taxol-stabilized microtubules. A single exponential fit to the residence time distribution (*A*, dashed line) was used to calculate the off-rate constant, k_{off}. A linear fit to the mean-squared displacement versus time-lag plot (*B*, dashed line) was used to determine the diffusion constant, D. Markers represent the mean ± SEM (*C*) Microtubule disassembly speeds were measured in the presence of 500 pM wild-type (black bar, from Fig. 2*C*) or 500 pM 9A (green bar, *n* = 35) Ndc80 complex. Error bars represent SEM. Dashed horizontal line represents the intrinsic disassembly rate, 284 ± 15 nm/s, value reproduced from Fig. 2*C*. (*D*) Percentage of microtubules for which a curl was observed at the microtubule tip during disassembly in the presence of 500 pM wild-type (black bar, from Fig. 3*F*) or 500 pM 9A (green bar, *n* = 37) Ndc80 complex. Error bars represent counting uncertainties.

Table S1. Number of replicates for optical trap assays

Ndc80 complex	WT			9D			ΔN		
Concentration (nM)	0.5	1	5	5	10	20	5	10	20
n (Disassembly-tracking fraction)	40	84	74	98	134	58	122	111	74
n (Disassembly speed)	21	47	54	8	46	53	11	39	40
n (Number of rescues)	2	15	32	ND	0	3	ND	3	15
Rescue rate observation time (minutes of disassembly)	5	14	14	ND	16	29	ND	13	26

ND, not determined.
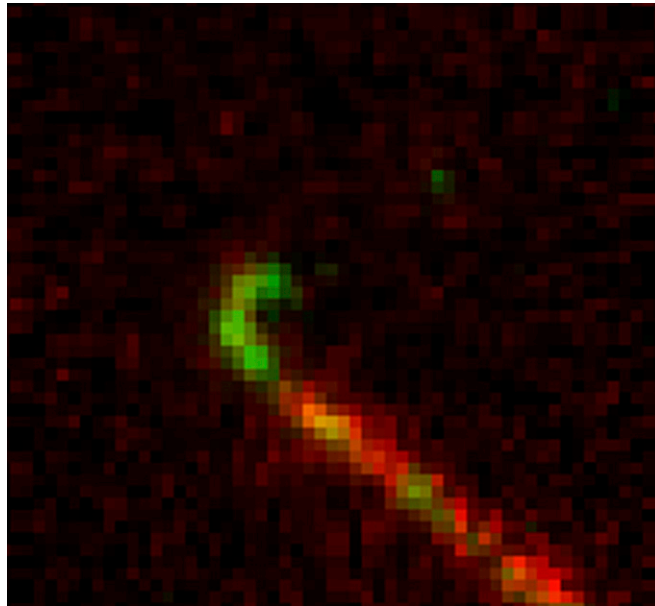
Movie S1. Ndc80 complex stabilizes curled extensions at disassembling microtubule tips. Movie shows 500 pM GFP-tagged Ndc80 complex (green) on a disassembling Alexa-647-labeled microtubule (red). GFP and Alexa-647 channels were visually aligned, and the brightness and contrast were adjusted for clarity using custom Labview software. Movie dimensions are 6.5 by 5.9 μm, and playback is at 9× speed.

Movie S1